

OPEN ACCESS

EDITED BY

Chamindra L. Vithana,

Southern Cross University, Australia

REVIEWED BY

Qiming Sun,

Xi'an University of Architecture and Technology,

China

Yingzhi Qian,

Wuhan University, China

*CORRESPONDENCE

Chaoqun Chen,

□ chenchaogun@mail.cgs.gov.cn

doi: 10.3389/fenvs.2025.1614178

RECEIVED 18 April 2025 ACCEPTED 26 August 2025 PUBLISHED 10 September 2025

CITATION

Dai H, Fang Y, Chen C, Liu K, Li X, Yang Z, Fang N and Zhang Y (2025) Geochemical evaluation and driving factor analysis of soil salinization in Northeast China Plain.

Front. Environ. Sci. 13:1614178.

COPYRIGHT

© 2025 Dai, Fang, Chen, Liu, Li, Yang, Fang and Zhang. This is an open-access article distributed under the terms of the Creative Commons Attribution License (CC BY). The use, distribution or reproduction in other forums is permitted, provided the original author(s) and the copyright owner(s) are credited and that the original publication in this journal is cited, in accordance with accepted academic practice. No use, distribution or reproduction is permitted which does not comply with these terms.

Geochemical evaluation and driving factor analysis of soil salinization in Northeast China Plain

Huimin Dai^{1,2,3}, Yunting Fang^{2,4}, Chaoqun Chen^{1,2,3}*, Kai Liu^{1,2,3}, Xiao Li¹, Ze Yang^{1,2,3}, Nana Fang^{1,2,3} and Yihe Zhang^{1,2,3}

¹Shenyang Center of China Geological Survey, China Geological Survey Shenyang Center, Shenyang, China, ²Key Laboratory of Black Soil Evolution and Ecological Effect, Ministry of Natural Resources, Shenyang, China, ³Key Laboratory of Black Soil Evolution and Ecological Effect, Shenyang, China, ⁴Shenyang Institute of Applied Ecology, Chinese Academy of Sciences, Shenyang, China

Introduction: The Songnen Plain in Northeast China is considered as one of the world's three major saline-alkali land regions. However, the evaluation of the extent and degree of saline-alkali land has primarily been mainly obtained via remote sensing interpretation, leading to inconsistencies in data on salinization levels and the area of saline-alkali land.

Methods: Random Forest-based modeling of total salt-exchangeable cation-chemical composition relationships facilitated high-precision spatial evaluation of soil salinization across Northeast China Plain.

Results: The results show that: (1) Northeast China contains approximately 16.93 million hectares of salinized or alkalinized zonal soils, where pH and salinity levels demonstrate statistically significant positive correlations (p < 0.01) with concentrations of chloride (Cl), sodium (Na), magnesium (Mg), calcium (Ca), sulfur (S), and potassium (K). (2) Northeast China's Songliao Plain contains 6.92 million hectares of saline-alkali soils, exhibiting a distinct spatial gradient in soda salinization chemistry: from sulfate-dominated in the northeast, transitioning through chloride-sulfate composite zones, to carbonate and finally chloride-dominated types in the southwest. (3) Chloride and bicarbonate dominate the saline-alkali soils, primarily distributed in low plains (<200 m elevation) with distinct spatial zonation. (4) Since the 1980s, strongly alkaline soils (pH > 9.5) have expanded by 80,300 ha/year, accompanied by significant organic matter and nitrogen depletion.

Discussion: Research indicates that integrated topography-hydrogeology-climate factors drive soil salinization, while consistent and stable farming practices can mitigate its progression.

KEYWORDS

random forest modeling, soil salinization, geochemistry, saline-alkali soil, Northeast China Plain

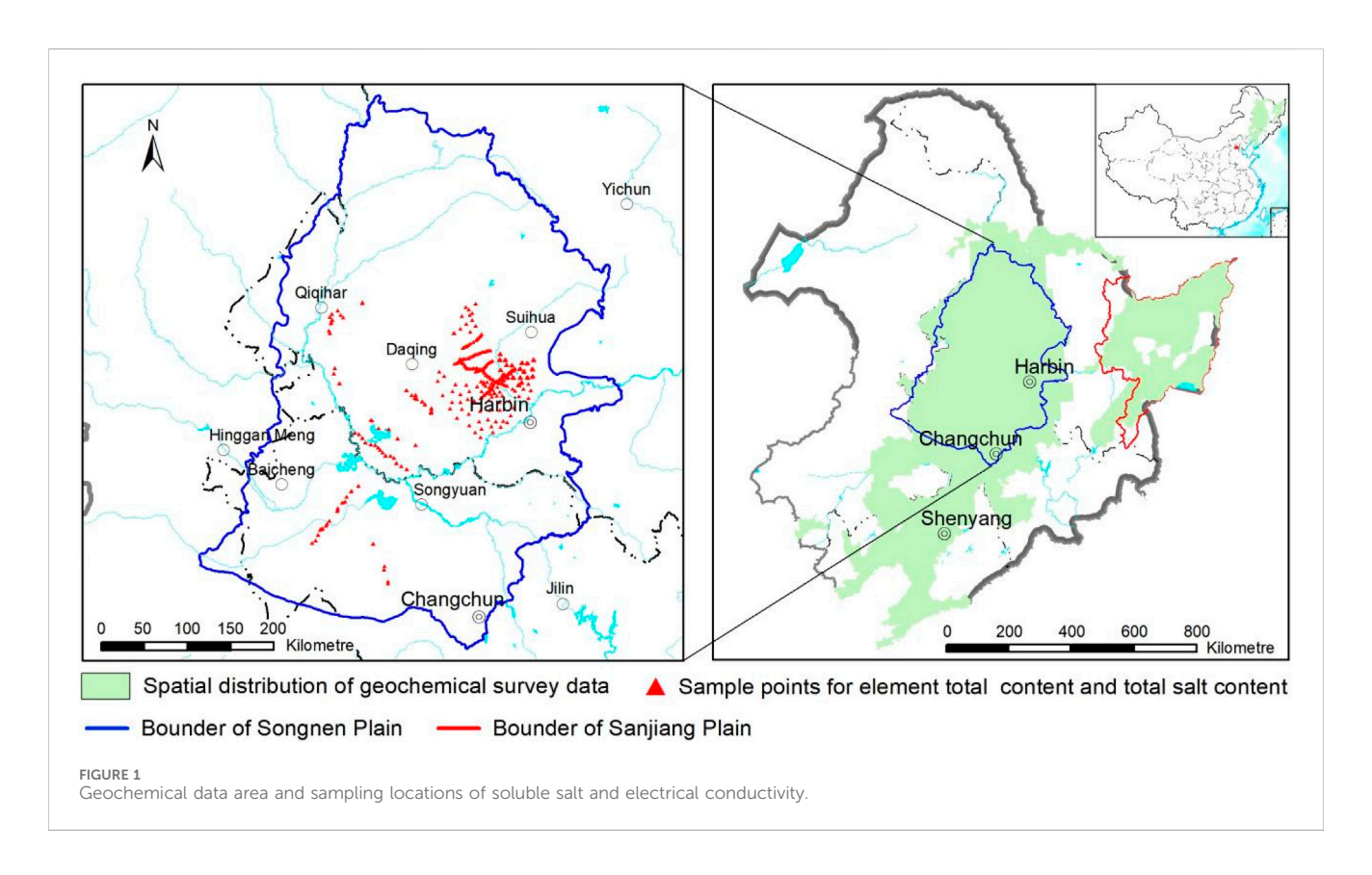
1 Introduction

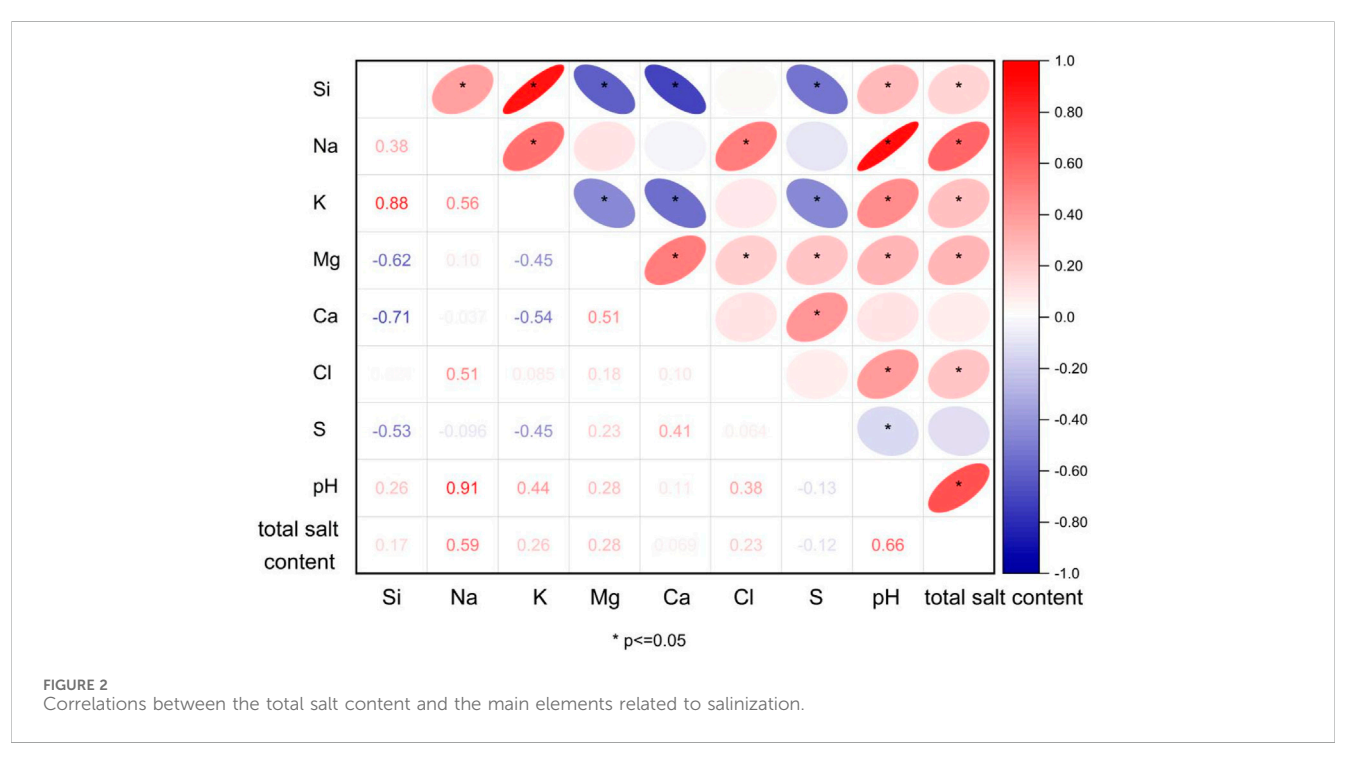
Soil salinization poses a multifaceted threat to global agriculture through three primary mechanisms. First, elevated salt concentrations directly impair crop productivity, currently affecting 833 million hectares of arable land and causing \$27.3 billion in annual losses (FAO, 2022). Second, high salinity and pH ($8 \le pH < 10$) degrade soil structure, reduce fertility,

and disrupt element cycling (Xing et al., 2024; Liu et al., 2024), beyond species-specific thresholds, salinity causes linear yield declines (Corwin, 2021), with pH > 8.5 rendering soils increasingly inhospitable (Liu et al., 2024). Third, high salinity exerts far-reaching impacts on the ecological environment, including exacerbating soil organic carbon loss to undermine ecosystem services and intensifying land degradation that threatens agricultural sustainability (Chen et al., 2025), salt stress causes decrease in plant growth and productivity by disrupting physiological processes (Sudhir and Murthy, 2004). This crisis is accelerating due to climate change (decreased precipitation) and poor irrigation practices, expanding salt-affected areas by 1,060.1 million hectares globally (Eswar et al., 2021; Tedeschi, 2020; Kirsten et al., 2018; Tedeschi, 2020). Secondary salinization now threatens 20% of irrigated lands (Li et al., 2024), with projections suggesting 50% of croplands may be affected by 2050 (Wang et al., 2003; Singh, 2021; Butcher et al., 2016; Daliakopoulos et al., 2016). However, as highlighted in FAO's 2021 global assessment, substantial uncertainties persist regarding three critical parameters: total affected area quantification, spatial distribution patterns, and soil quality characterization (FAO, 2022). The assessment of global saline-alkali land area and its hazards remains uncertain due to methodological variations in salinity measurement (Lobell, 2010; Lobell et al., 2010; Corwin, 2021; Ivushkin et al., 2019).

Soil inorganic minerals, formed through rock weathering and sedimentation processes, exhibit systematic redistribution governed by thermodynamic principles (Xu and Xu, 2018; Zhang and Feng, 2009). This geochemical process adheres to the lowest free energy principle, inducing spontaneous element migration from high to low chemical potential zones until thermodynamic equilibrium is achieved (Wang and Huang, 2023). In open geochemical systems, rock weathering facilitates multidirectional element migration, including both vertical leaching and lateral transport (Hao et al., 2004; Zhao et al., 2019). Hydrodynamic forces in shallow cover regions significantly influence element redistribution. Notably, inland depressions emerge as key geochemical reactors where inorganic mineral elements undergo sequential redistribution, migration, precipitation, and accumulation. The precipitation behavior and mobility of major ions (Na+, Mg2+, K+, Ca2+, Cl-, SO42-) in these depressions demonstrate strong correlations with their ionic radii, valence states, and crystalline lattice stability (Zhang et al., 2010; Thorne, 1954). These elements, originating from local parent materials, experience complex transformation pathways through gravitational settling and hydrological cycling, ultimately manifesting as residual primary minerals, secondary clays, or dissolved salts species (Dai et al., 2022; Eswar et al., 2021). The salinization mechanism involves solute transport to root zones with limited leaching (Adeyemo et al., 2022), particularly in arid regions where evaporation exceeds precipitation (Nachshon, 2018). Spatial salt accumulation patterns reflect complex hydrogeochemical interactions, with NaCl, Na2SO4 and carbonate minerals dominating in typical inland basins (Chaieb et al., 2019), as exemplified by the well-documented hydromorphic salinization phenomena in Tuva region (Chernousenko and Kurbatskaya, 2017). These comprehensive findings highlight the critical necessity for developing advanced monitoring techniques and implementing effective mitigation strategies to address soil salinization challenges. Salt element content critically influences soil pH, a key salinization indicator (Muhammad et al., 2024). While NaCl dominates saline soils (Rengasamy, 2016), comprehensive soil characterization (mineralogy, texture, chemistry) remains essential for effective amendment selection (Elmeknassi et al., 2024).

In recent years, soil salinization prediction has transitioned from traditional empirical models to data-driven paradigms, with machine learning (ML) progressively evolving through the integration of multi-source remote sensing data and ground observations; recent studies widely adopt a "satellite remote sensing (Sentinel-2/Landsat) + UAV multispectral + ground sensors" tri-level data synergy modeling approach to enhance salinization prediction accuracy (Wang et al., 2024), such as Bayesian Neural Network models applied in China's Yinchuan Plain, multi-model fusion in inland arid regions (Wang L. et al., 2023), and Partial Least Squares Regression (PLSR) models in coastal salinization zones of India (Kumar et al., 2024), however, remote sensing interpretation of soil salinization cannot reflect deep-layer salt distribution nor detect certain obscured saltmasking information in soils. Geospatial analysis reveals that the salinization land concentrated distribution across four key regions in China: the Songnen Plain, northwestern arid/semiarid zones, Yellow-Huaihai Plain, and eastern coastal areas (Wan et al., 2019; Zhang et al., 2017). Existing research on soil salinization in the Songnen Plain has primarily relied on remote sensing interpretation methods (Dai et al., 2022) and limited profile data, with reported affected areas ranging from 3.42 to 5 million hectares showing considerable variation (Xu et al., 2018; Hu et al., 2023; Wang et al., 2014; Zhang and Feng, 2009; Zhao and Jia, 2020; Chen et al., 2020), remote sensing interpretation is only an indirect inversion method and is greatly influenced by the data quality, models, and personnel experience (Eswar et al., 2021), resulting in each employing distinct methodologies that yield inconsistent results. The Songnen Plain in Northeast China represents a typical soda saline-alkali land characterized by distinctive NaHCO₃/Na₂CO₃ salt composition and marked spatial heterogeneity (Xu et al., 2018; Wang J. et al., 2023), creating unique monitoring challenges that exceed the capabilities of conventional assessment methods. In the 1950s, mild salinization was the main form of salinization, while by 2001, moderate to severe salinization had become the predominant form (Zhang et al., 2010; Lin and Tang, 2005; Wang et al., 2019). The targeted regional surveys have not yet been carried out, and the amount of high-precision soluble salt data for this region is insufficient and lacks wide coverage. Based on the massive existing measured data of soil geochemistry in Norteast China, employing state-of-the-art machine learning technologies to assess salinization conditions can bridge the gap in systematic salinization surveys. This study leverages high-resolution geochemical data to: 1) establish soil composition-salinization relationships, 2) map salinization patterns in Northeast China, 3) enhance global mapping accuracy, and 4) constrain a comprehensive insight into the salinization evolutionary characteristics and formation mechanism in Northeast China, ultimately informing targeted remediation strategies.





2 Materials and methods

2.1 Study area

Northeast China Plain encompasses the Songliao Plain (comprising the Songnen Plain and Liaohe Plain) and the

Sanjiang Plain. The Songliao Plain, spanning approximately 3.5 million hectares, occupies a strategic position between the Greater Khingan Mountains (Da Hinggan Ling), Lesser Khingan Mountains (Xiao Hinggan Ling), and Changbai Mountains. This U-shaped lowland formation primarily results from alluvial deposition by the Songhua, Nenjiang, and Liao Rivers, creating

TABLE 1 Importance of soil pH to major chemical indexes.

Indexes	Importance	Importance of normalization (%)		
Al	0.086	35.5		
Ca	0.063	26.2		
Cl	0.113	46.8		
Organic carbon	0.056	22.9		
Fe	0.039	15.9		
I	0.063	25.9		
K	0.049	20.1		
Mg	0.103	42.3		
Na	0.242	92.0		
S	0.104	43.0		
Si	0.082	34.0		

an expansive, gently undulating terrain with well-developed hydrological systems. The plain's unique geological structure comprises three distinct geomorphic units: the eastern high plain, central low plain, and mountain-front inclined plain. Situated in a temperate transitional zone between semi-humid and semi-arid climates, the region experiences a continental monsoon climate characterized by seasonal variations: windy, dry springs; hot, rainy summers; variable autumn conditions; and cold, relatively snow-free winters. Annual precipitation (400-600 mm) is significantly exceeded by evaporation rates (1000-1800 mm), creating distinct hydrological challenges. The surrounding mountainous regions (Greater Khingan, Lesser Khingan, and Changbai Mountains) feature volcanic, intrusive, and metamorphic rock formations. Hundreds of rivers originating from these highlands transport various salts to lower elevations, creating dynamic material migration patterns that have shaped the plain's diverse soil composition. Dominant soil types include phaeozem, chernozem, dark brown soils, and meadow soils, with distinct spatial distribution patterns: chernozem and meadow soils in low-lying areas; black and dark brown soils at higher elevations; aeolian sandy soils in southwestern regions; and saline-alkali soils concentrated in the central hinterland. Notably, the Songnen Plain contains one of the world's three major soda saline-alkali-soil distribution areas and China's largest such region. The Sanjiang Plain (108,900 km²), formed by alluvial deposits from the Heilongjiang, Ussuri, and Songhua Rivers, completes this important geographical system. Since the mid-20th century, compounding factors including global climate change, rapid population growth, and intensive land use have accelerated environmental challenges, particularly soil salinization and grassland degradation in the Songliao Plain region.

2.2 Sample collection

Soil samples were systematically collected from the topsoil layer (0–20 cm) using a standardized grid-based sampling methodology collected at a density of 1 point/km². During sample collection,

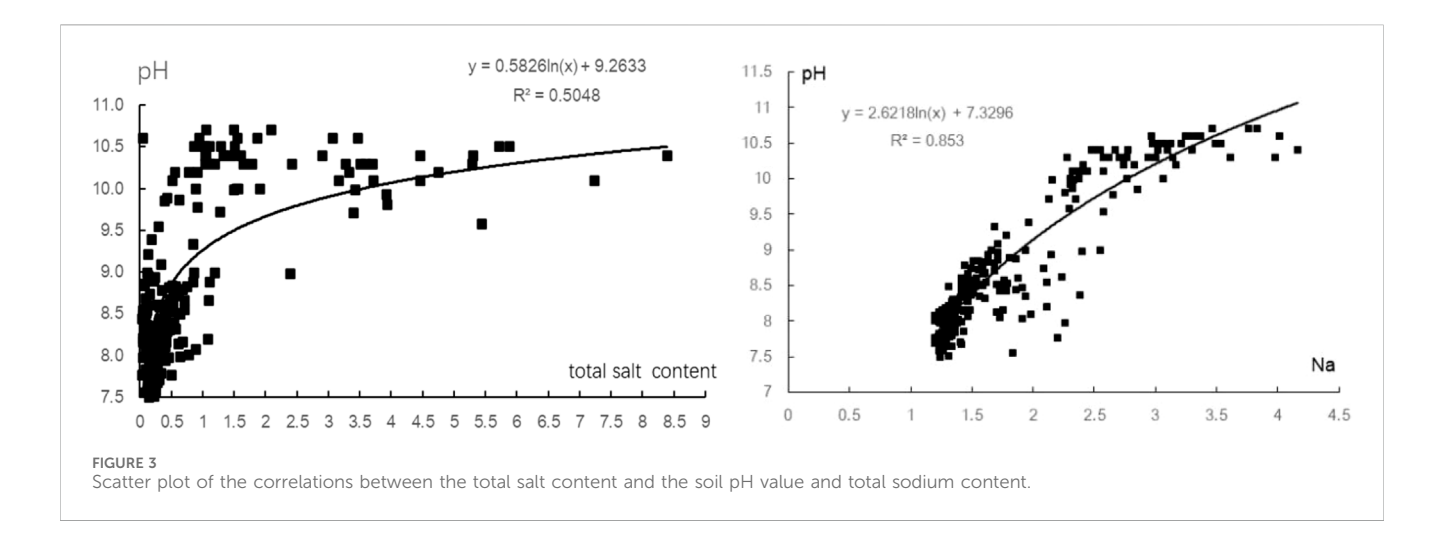
surface debris was removed, and every three soil points were mixed to create one soil sample, and soil samples from each 4 km² were combined for testing chemical total content. The collected and analyzed samples provide comprehensive coverage of both the Songliao and Sanjiang Plain (Figure 1). To establish relationships between total soil chemical composition and basic ions/salt content for digital mapping of soil salinization, 407 surface soil samples were collected in the core zone of the Songnen Plain. The sample collection protocol followed the same method used earlier. Soil pH data of the 1980s were obtained from The Second National Soil Census (Shi et al., 2010).

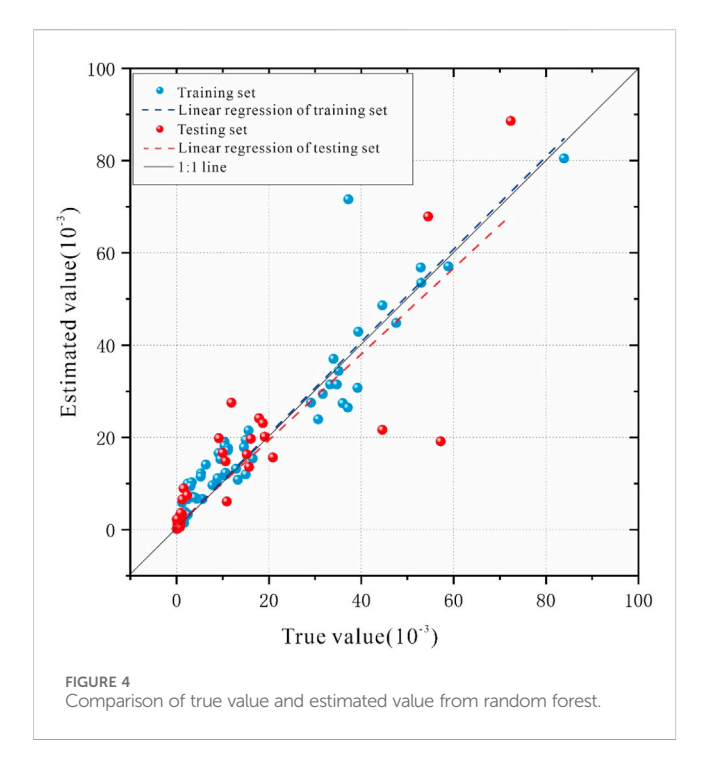
Geochemical characterization was conducted using rigorous analytical protocols to assess soil properties across the Northeast China Plain. Total elemental contents and pH were analyzed through standardized methods: X-ray fluorescence spectrometry for Ca, Cl, Mg, Fe, K, Na, P, Si and Al; glass electrode measurement for pH; volumetric analysis for organic carbon and N, and Inductively Coupled Plasma Mass Spectrometry for I. All analyses were conducted within a concentrated timeframe with strict quality control measures, including randomized batch processing of samples, controls, and reference materials (12 GBW Standards per 500 samples), achieving 100% accuracy in validation. A total of 407 surface soil samples underwent comprehensive analysis of total elements (Si, P, Al, Fe, Na, K, Mg, Ca, Cl, N, Total Carbon, Organic Carbon, S and I), ionic species (Mg²⁺, Ca²⁺, Na⁺, K⁺, Cl⁻, SO₄²⁻, CO₃²⁻ $, HCO_3^-, PO_4^{3-}), and physicochemical parameters (pH, total salinity,$ EC). Ion chromatography (Dionex ICS-5000+) quantified soluble salts, while the standardized electrode method (GB/T 15496-2017) measured EC at 25°C using electrical conductivity of the saturated soil extract.

2.3 Selection of prediction model

Statistical analysis of the 407 soil samples demonstrated significant linear relationships between total soluble salts and salinization-associated elements (Figure 2). The total salt content showed statistically significant positive correlations (*p \leq 0.05) with pH and Na with coefficients of 0.57 and 0.61 respectively, as well as with Mg, Ca and Cl concentrations, with sodium and pH exhibited the strongest associations with salinity levels. Notably, pH and Na displayed particularly strong intercorrelation (r = 0.69), suggesting their combined utility as reliable indicators of salinization intensity. Parallel analysis revealed an equally strong positive correlation between K and Si (r = 0.69), which may reflect desertification processes through potassium silicate weathering patterns. These consistent correlation patterns collectively demonstrate that elemental composition analysis provides a robust methodological framework for monitoring and assessing soil salinization dynamics across the Northeast China Plain.

Statistical evaluation of chemical component contributions to pH normalization in saline-alkali soils demonstrated that Na, Cl, Mg, and S collectively accounted for over 40% of pH variation (Table 1). These findings confirm that these elements, along with Na, Cl, Ca, Mg, serve as reliable salinization indicators. Furthermaore, the strong predictive relationships support the development of quantitative models using total soluble salts to classify both the intensity and typology of soilsalinization.





The scatter plot analysis of pH *versus* total sodium and total salt content (Figure 3) revealed a non-linear relationship between these parameters. This suggests that traditional linear regression models struggle to accurately predict the total salt content index. The random forest algorithm, introduced by Breiman in 2001, is an effective machine learning method. Built upon an ensemble learning framework that utilizes decision trees, random forest is particularly well-suited for addressing nonlinear problems (Breiman, 2001). The algorithm not only demonstrates excellent resistance to noise interference and robustness to missing data, but also maintains a high level of prediction accuracy. Moreover, a significant advantage of the random forest is its capacity to assess feature importance, thereby enabling the direct quantification of each variable's contribution to the prediction target. This characteristic greatly enhances the interpretability of the model.

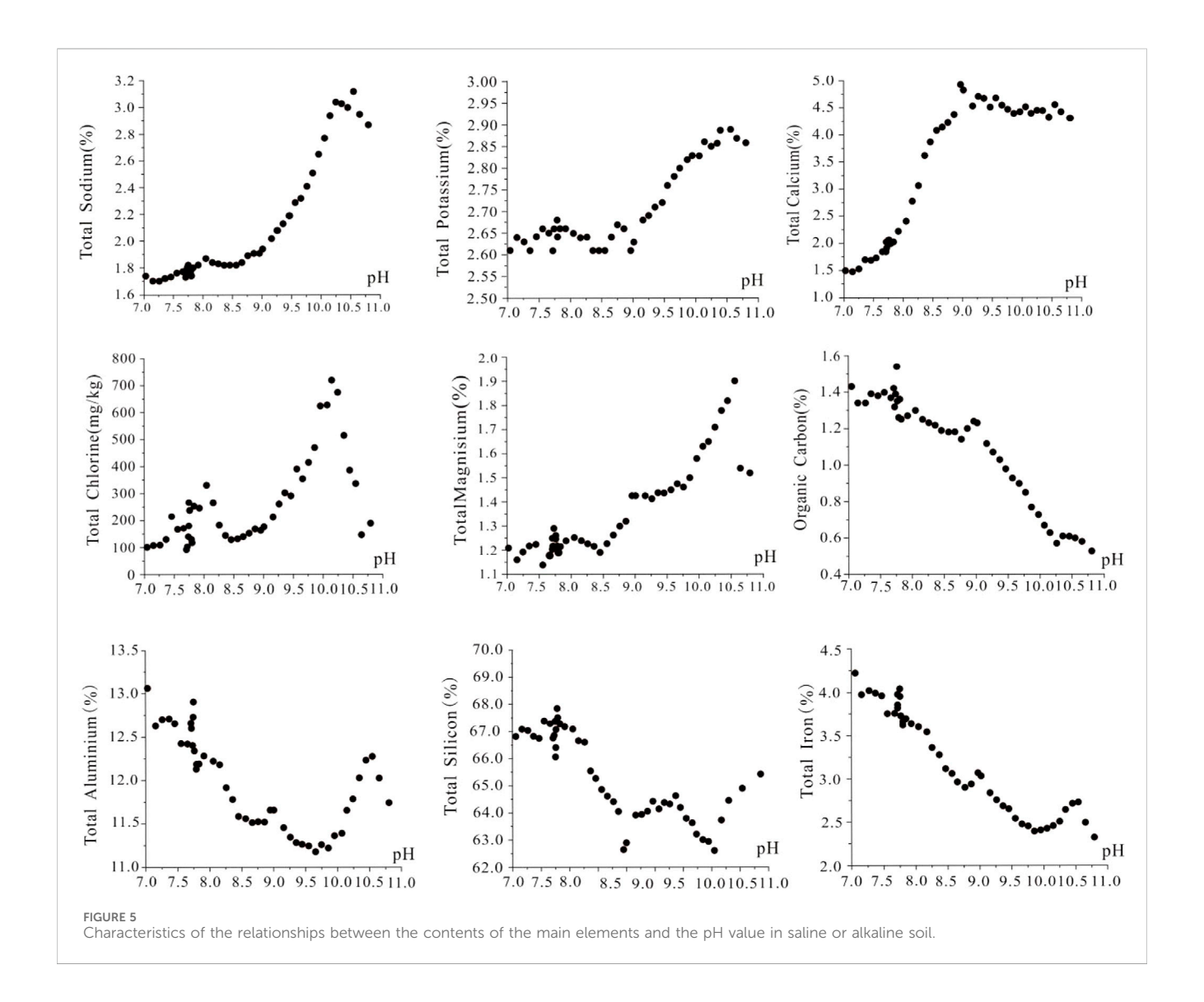
To accurately characterize the complex relationship between elemental composition and salinization-related salt content, the random forest algorithm was employed to model the soil salinityelement relationships. The optimization process involved outlier removal (X±3σ) from the initial 407 samples, resulting in 389 quality-controlled samples for model development. The training set and testing set were divided in 70:30. The random forest model was constructed using pH, Na, K, Mg, Ca, Si, S, and Cl as input features, with the total salt content serving as the dependent variable. Each random forest comprises 500 regression trees. One-third of the predictor variables are randomly selected for constructing each tree in order to reduce inter-tree correlation. The accuracy of the model was evaluated using the R^2 coefficient of determination (R^2) and Root Mean Square Error (RMSE) metrics. As illustrated in Figure 4, the random forest model demonstrates high predictive accuracy and exhibits a satisfactory fitting performance on both the training set (Table 2). This suggests that it can effectively capture the intrinsic relationship between soil element composition and total salt content, thereby making it applicable to predictive studies of total salt content distribution in soil. These optimized models were successfully applied to 42,306 spatial data points, enabling high-resolution mapping of salinization patterns across the Northeast China Plain. The methodology effectively captured the observed non-linear relationships while maintaining computational efficiency through the chosen parameter configuration.

2.4 Classification method

The scatter plot analysis (Figure 5) of soil elemental mean contents (Ca, Mg, K, Si, Fe, Al) at 0.1 pH intervals revealed multiple inflection points in element-pH relationships at pH 8.0, 8.5, 9.0, and 10.0. Within the pH range of 8.5–9.0, the concentrations of K, Na, and Cl exhibit a gradual increase following a stable phase in their scatter plots against pH, when pH exceeds 9.0, their concentrations demonstrate an accelerating trend. An inflection point was observed in the dispersion slope of each element at a pH of 9.0. Calcium showed contrasting behavior—its content rose

TABLE 2 Statistics of the training set, testing set, and model accuracy.

Index		Statistics					Model accuracy	
		Number	Maximum (10 ⁻³)	Minimum (10 ⁻³)	Average (10 ⁻³)	R²	RMSE (10 ⁻³)	
Total salt content	Training Set	285	83.9	0.046	3.9	0.9223	2.9249	
	Testing Set	122	72.4	0.062	3.65	0.7684	5.0629	
Cl-	Training Set	285	4.97	0.005	0.08	0.9404	0.22	
	Testing Set	122	3.49	0.001	0.064	0.7993	0.772	
SO ₄ ²⁻	Training Set	285	1.84	0.001	0.075	0.8849	0.1030	
	Testing Set	122	1.22	0.001	0.103	0.4766	0.1394	

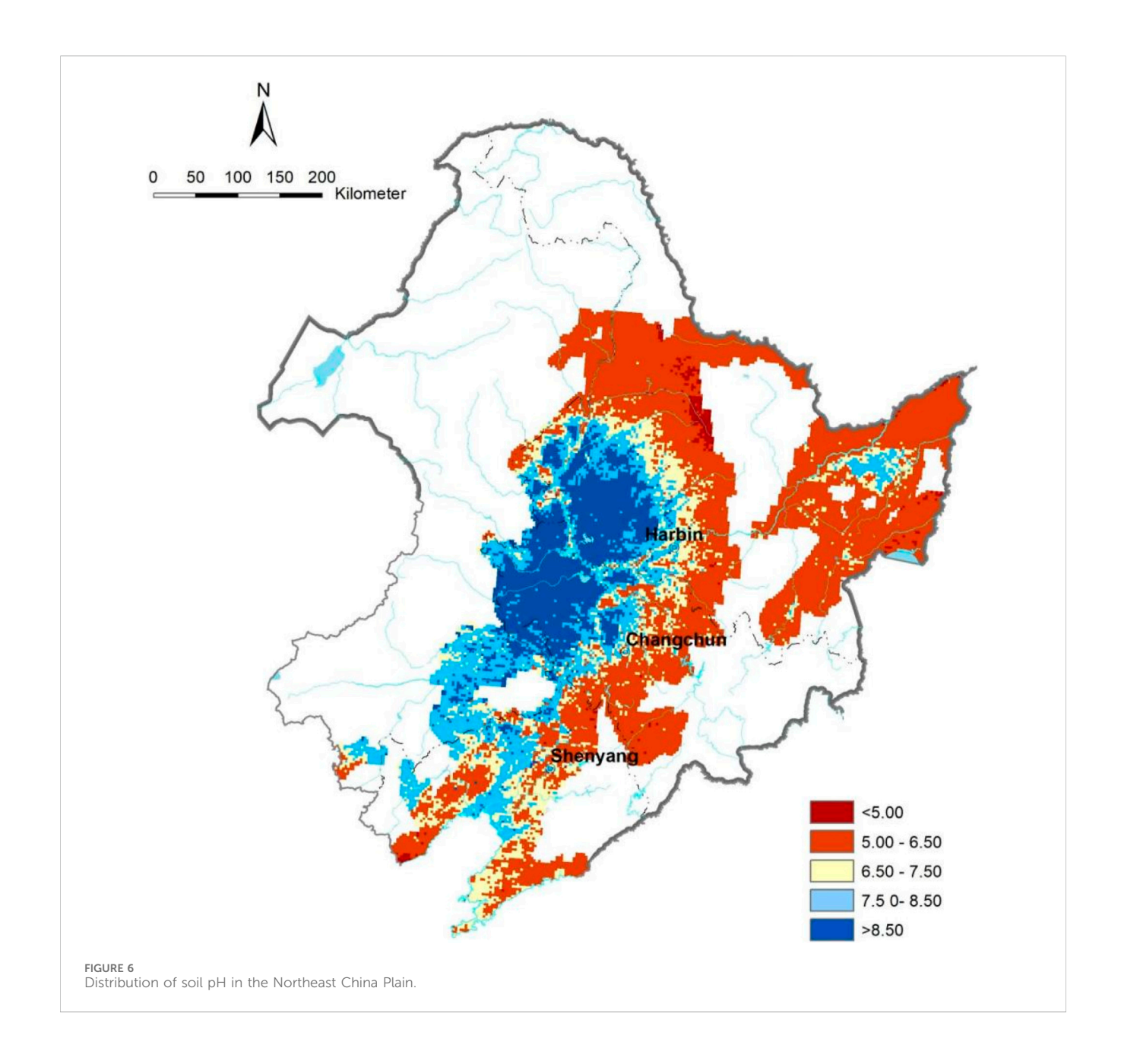


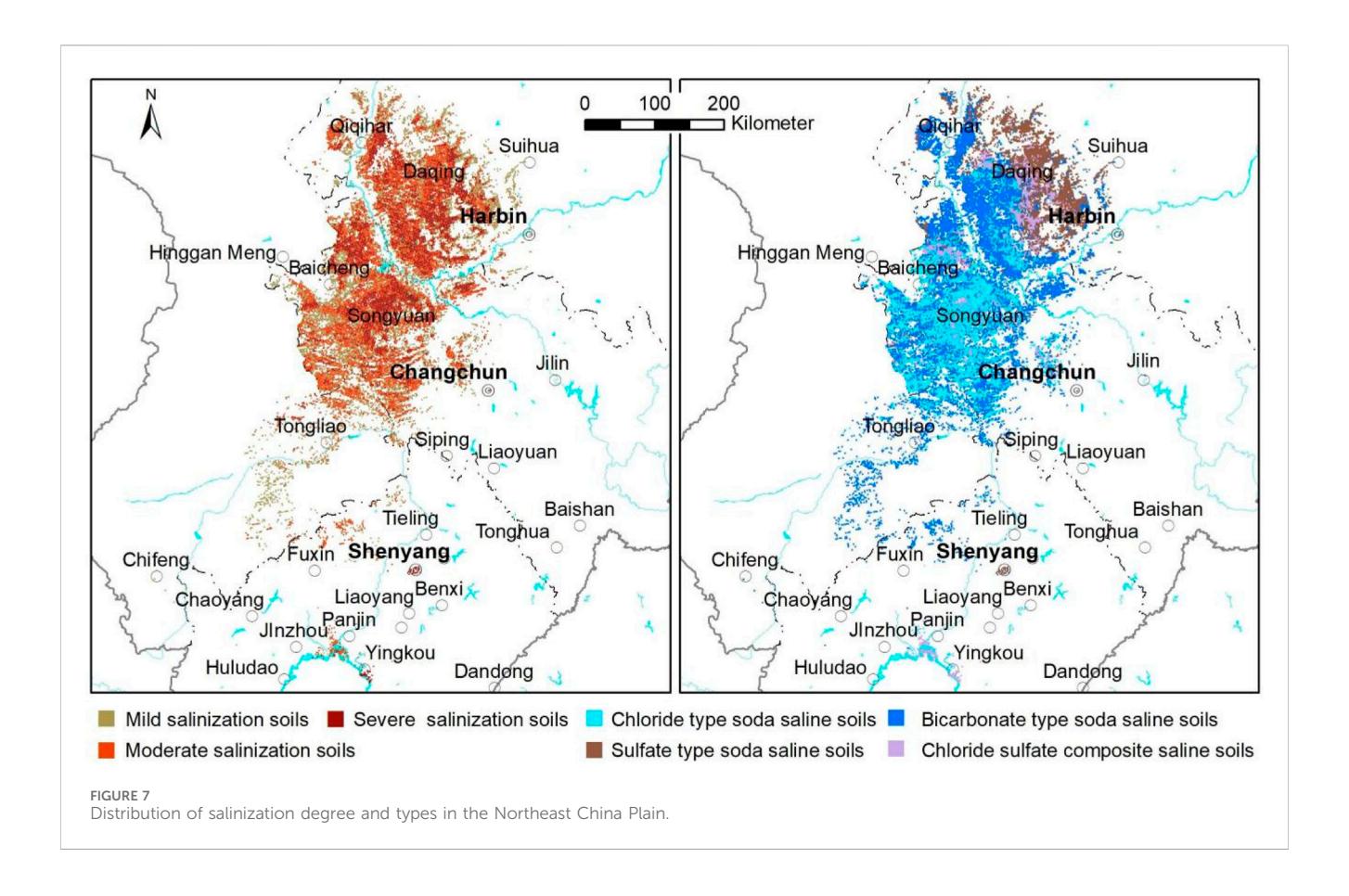
sharply below pH 8.5 but stabilized above pH 9.0, suggesting diminishing pH influence. Magnesium displayed biphasic accumulation, accelerating between pH 8.5-9.0 and again above

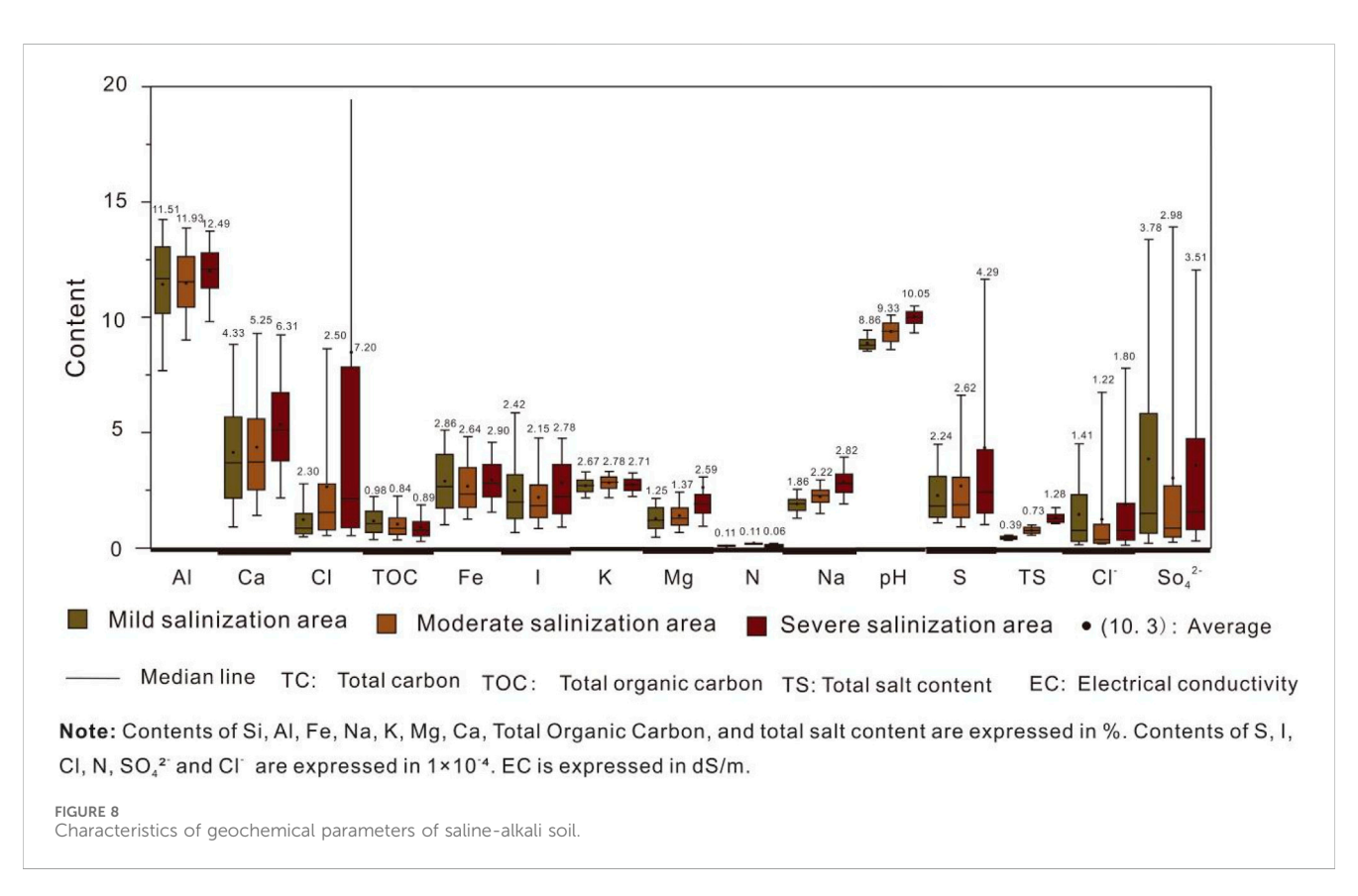
10.0, and contents of Na, Cl, Mg, and K declined variably beyond pH 10.0. Silicon and aluminum, as soil texture proxies, demonstrated pH-dependent trends: higher concentrations below

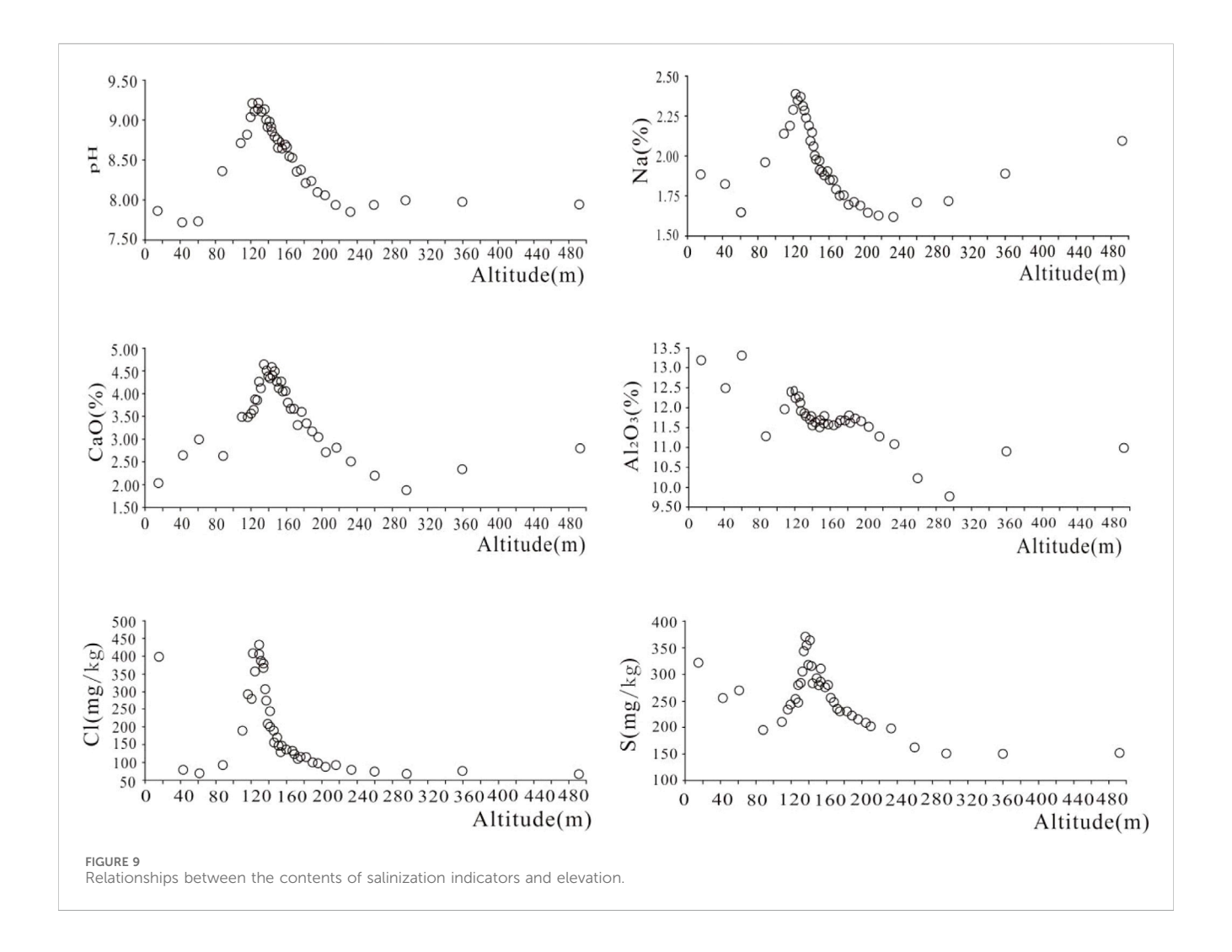
TABLE 3 Index system and limit values of salinization classification.

Salinization grade index and limit value			Salinization classification index and limit value			
Total salt content (%)	рН	Classification of salinization degree	Cl ⁻	SO ₄ ²⁻	Salinization type	
0.3-0.5	≥8.5	Mild salinization	≥0.4	≥0.5	Complex type	
0.5-1.0	≥8.5	Moderate salinization	≥0.4	≤0.5	Chloride type	
>1.0	_	Severe salinization	≤0.4	≥0.5	Sulfate type	
			≤0.4	≤0.5	Bicarbonate type	









pH 8.0, sharp decreases through pH 10.0, then abrupt recovery at 10.0–10.5. Their combined profile effectively tracks aeolian desertification and salinization processes. The evolving geochemical signatures delineate pH 8.5–9.0 as a decisive inflection point that triggers significant compositional shifts in key soil constituents (particularly base cations). This pH range constitutes a critical transitional threshold in salinization-desertification continuum dynamics, with pH = 8.5 representing the minimum threshold for dominant salinization processes.

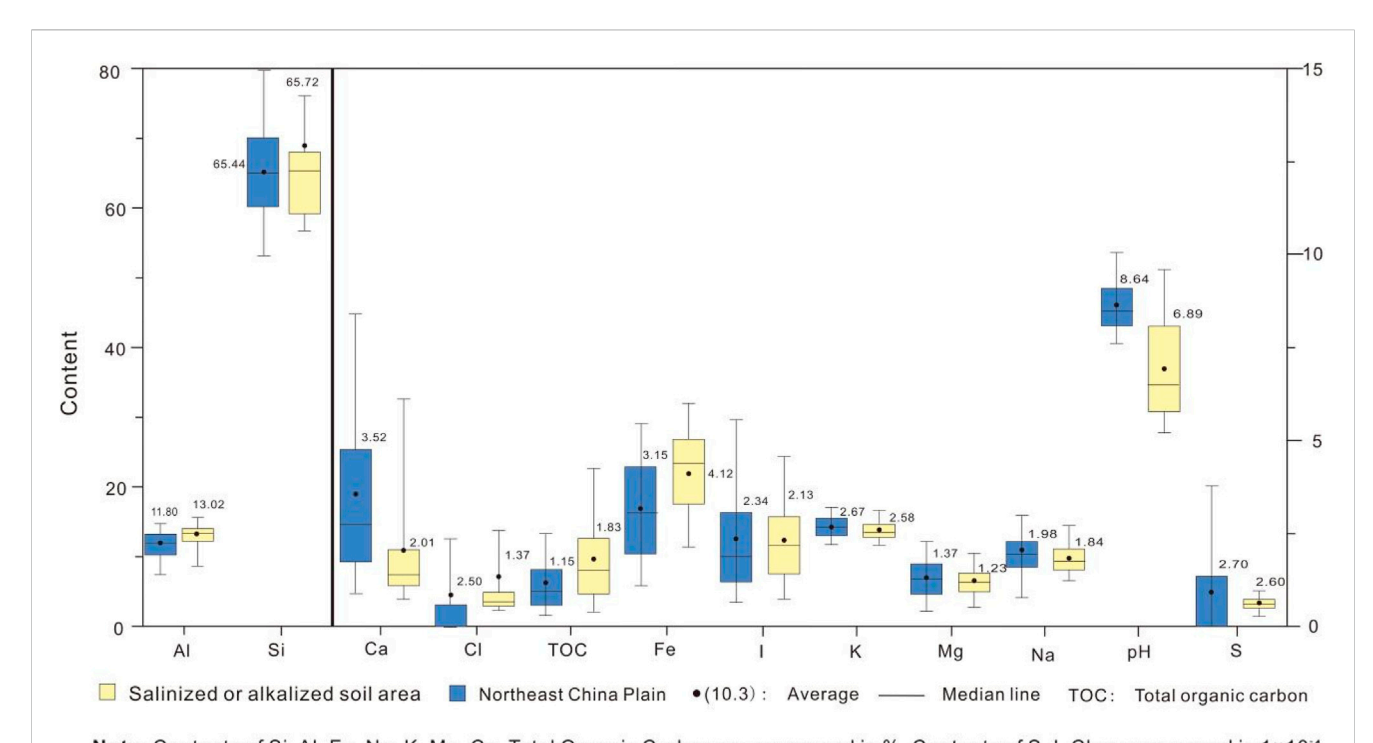
Based on the saline-alkali soil classification standards from the United States Salinity Laboratory (Daniels, 2016; Weil and Brady, 2016; Bao, 2000), and combining the characteristics of the soil's total salt content, chloride ion, and sulfate radical contents, relationship between base citation content, and other spatial data, we established a classification index system for the Northeast China Plain (Table 3). This system integrates geochemical parameters including total soluble salts, chloride ion (Cl⁻) and sulfate radical (SO₄²⁻) contents, pH values, and spatial distribution characteristics. Four types were divided: chloride-sulfate composite saline-alkali soil, chloride type saline-alkali soil, sulfate type saline-alkali soil, and bicarbonate type saline-alkali soil.

3 Results and discussion

3.1 Distribution and geochemical characteristics of saline-alkali soils

3.1.1 Characteristics of soil acidity and alkalinity

Our comprehensive soil analysis reveals distinct pH patterns across in China's Northeast China Plain, averaging 5.76 with marked spatial heterogeneity (Figure 6). Acidic soils (pH < 6.5) dominate 26.64 million hectares, primarily concentrated in the central-eastern Songliao Plain and most Sanjiang Plain regions, while strongly acidic soils (pH < 5.0) occupy 1.13 million hectares along the Lesser Khingan. The saline-alkali soils shows contrasting alkaline 42,306 with sampling points, covering 16.92 million hectares and an average pH of 8.63. These include chernozem, meadow soil, phenozem, aeolian sand soil, and salinealkali soils types, Regional analysis highlights the western Songliao Plain as a saline-alkali hotspot (16.47 million hectares, pH 8.65), comprising 8.23 million hectares of strongly alkaline soils (pH > 8.5) and 2.89 million hectares of extremely alkaline soils (pH > 9.5). The Sanjiang Plain's alkaline soils (457,200 ha) exhibit moderate alkalinity (mean pH 7.93, max 8.72). Land-use-specific analysis demonstrates that undeveloped saline-alkali lands maintain the



Note: Contents of Si, Al, Fe, Na, K, Mg, Ca, Total Organic Carbon are expressed in %. Contents of S, I, Cl are expressed in 1×10⁻⁴.

FIGURE 10 Characteristics of key chemical components and parameters related to salinization in soil.

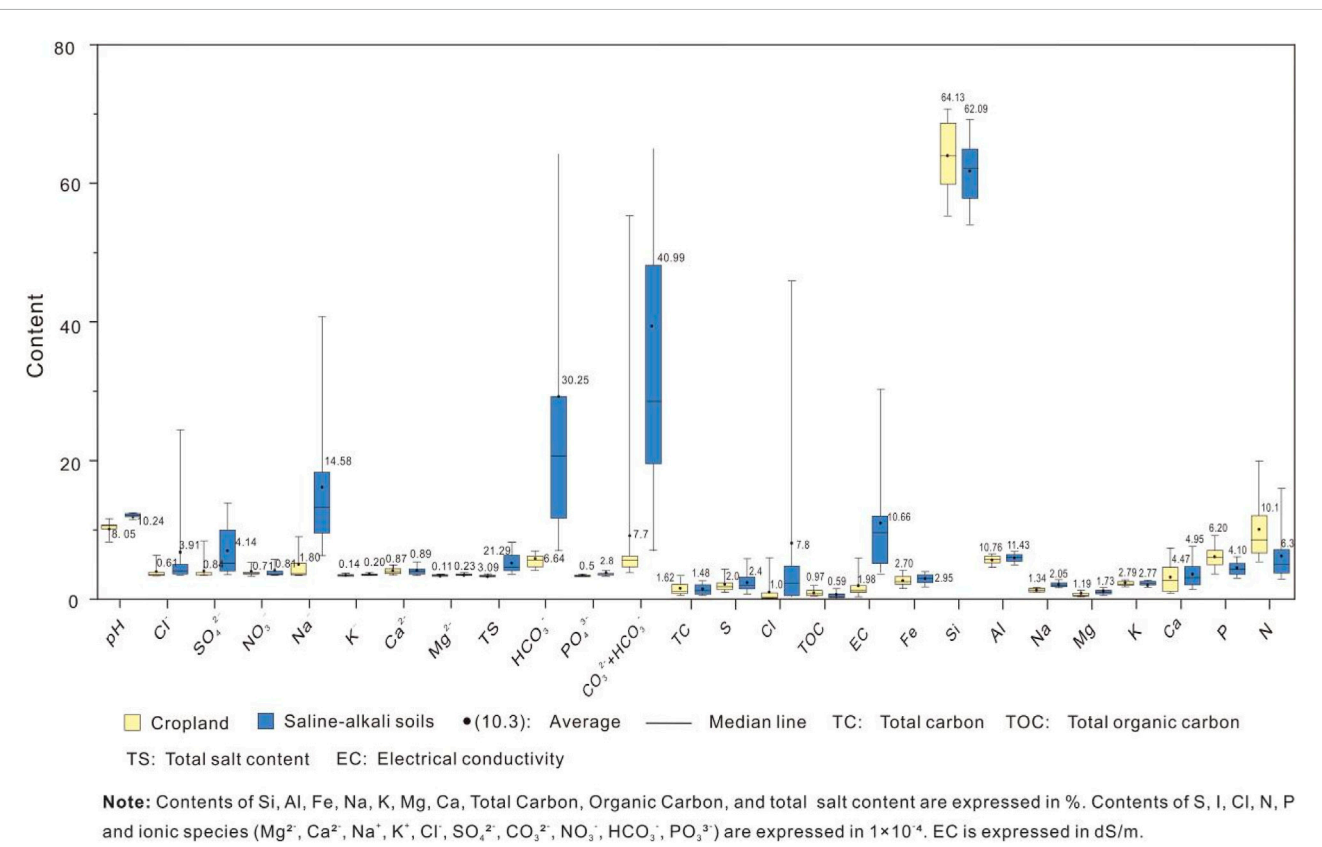
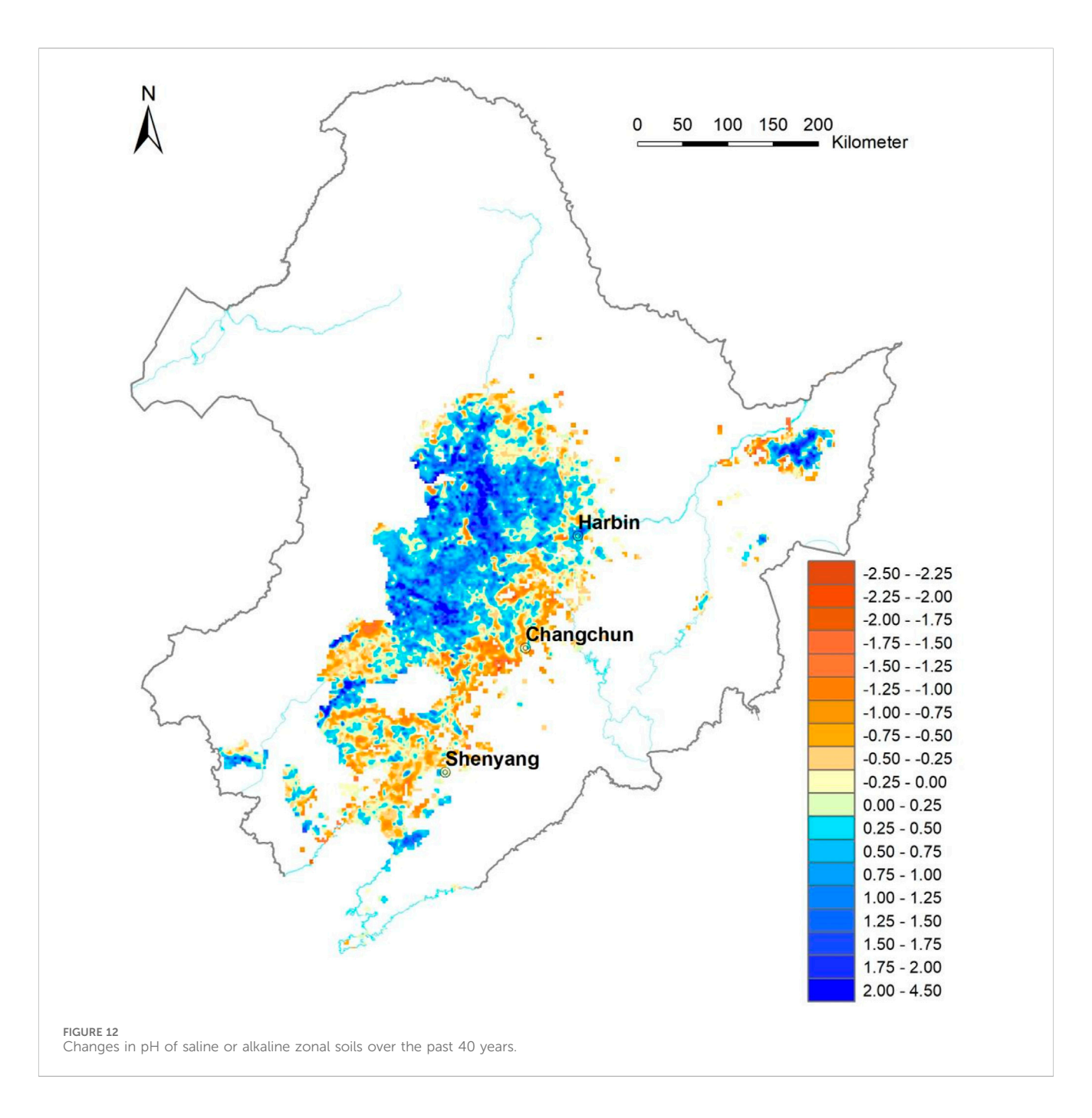


FIGURE 11 Parameter characteristics of ion and total content in saline-alkali soils.

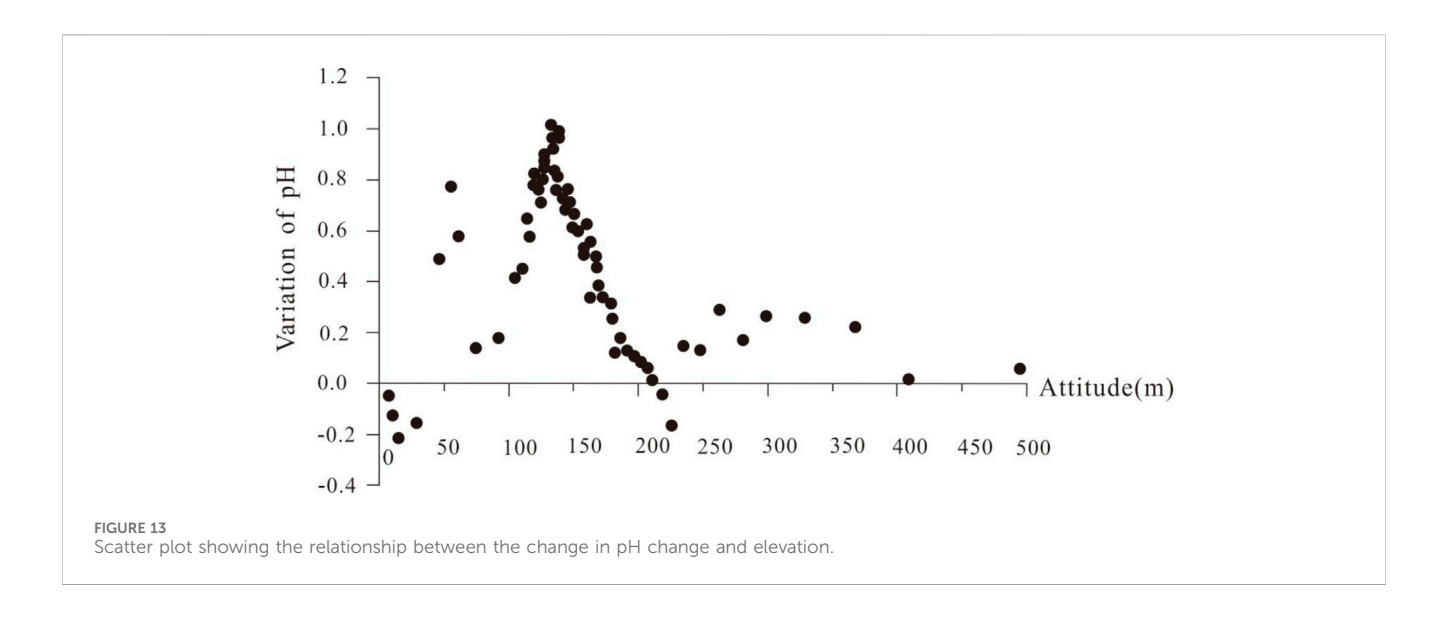


highest alkaline (pH > 9.0), followed by grasslands (pH 8.83) and swamps (pH 8.80), with pH values of 8.83 and 8.80, cultivated paddy and dry fields show relatively reduced alkalinity, with average pH values of 8.50 and 8.22, respectively.

3.1.2 Distribution of saline-alkali soils

The saline-alkali soils in the Northeast China Plain exhibit distinct spatial and geochemical patterns. Covering approximately approximately 6.92 million hectares, virtually all of these areas are distributed in the Songliao Plain's hinterland (Figure 7), these soils predominantly show mild (2.37 million hectares) and moderate (2.77 million hectares) salinization. with severe cases limited to 1.77 million hectares. The saline-alkali soils predominantly distribute in low-lying alluvial areas (<200 m elevation; mean

140 m)) in the Songliao Plain. A clear zonal distribution emerges from northeast to southwest (Figure 7), progressing from sulfate \rightarrow chloride-sulfate composite \rightarrow bicarbonate \rightarrow chloride types. Bicarbonate-type soils dominate (3.24 million hectares), followed by chloride-type (1.80 million hectares), while composite types are least extensive (1.16 million hectares), with chloride-rich variants concentrated in southern basins. Geochemical analysis (Figure 8) shows dynamic relationships: while Na, Ca, Mg, Cl and S contents increase linearly with salinization intensity, similar to the variation trends of total soluble salts, sulfate ions, and chloride ions with intensifying salinization. Chloride shows a parabolic trend (peaking 130 m elevation; Figure 9). The lowest average elevations coincide with moderate salinization zones, with pH and major cation concentrations peaking at 140 m elevation. These patterns reflect



ion migration dynamics in the plain's hydrogeochemical convergence zone, where multiple ions collectively influence salinization processes. Notably, increasing salinity correlates with elevated Al and depleted Si contents, alongside degraded soil structure and fertility, demonstrating the multifaceted impacts of salinization on pedogenic processes.

3.1.3 Geochemical characteristics

The saline-alkaline soil areas exhibited significantly higher concentrations of salinization-related elements (Ca, Na, Cl, K, S, and Mg) compared to those in the Northeast China Plain (Figure 10). In contrast, these areas showed lower levels of Al, Fe, organic carbon, and N relative to the Northeast China Plain. Silicon content remained comparable between both regions. Notably, the most pronounced differences were observed in the primary salinity indicators (Ca, Na, and Cl), which were substantially elevated in soils with pH > 7.5.

The geochemical parameters of the soil samples collected from salinized or alkalized zones revealed significant variations between cultivated land and saline-alkali land (Figure 11). The total contents of the salinization-related elements and base cations (median and average) were lower in the cultivated land than those in the saline-alkali land, and the Cl-, S, organic carbon contents, and pH values were significantly different between the two land types. The coefficients of variation for salinization indicators-including Cl-, Ca2+, Mg2+, Na+, K+, SO₄2-, total salt content, electrical conductivity, and the combined concentration of HCO₃⁻ and CO₃²⁻—were significantly higher in cultivated soils than in saline-alkali soils. In contrast, the spatial variability of nutrients and fertility indicators (organic carbon, total nitrogen, and total phosphorus contents) was significantly greater in the cultivated soils. The spatial variability of the base cations in saline-alkali soils was relatively weak, with the variation coefficient of Ca2+ content being the smallest (though still >0.6). These elevated variation cations suggest possible coefficients of base convergence phenomen.

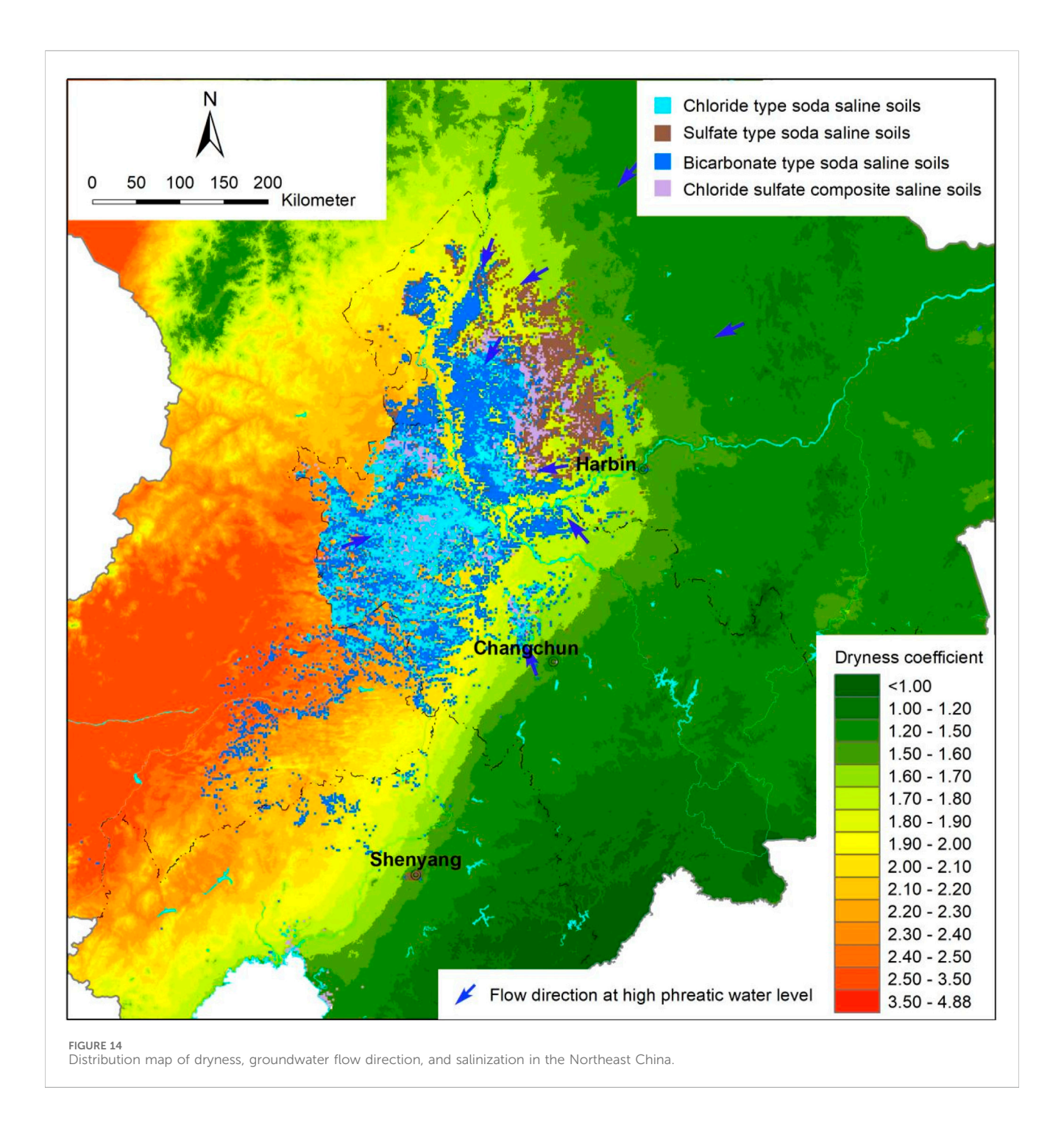
3.2 Spatiotemporal patterns and controlling factors of pH variation in saline-alkali soils

3.2.1 Spatiotemporal characteristics of pH values

This study utilizes pH variation as a proxy indicator for assessing soil salinization dynamics in China's Northeast China Plain over the past 4 decades, based on the positive correlation between pH and total salt content, and the absence of high-resolution spatial data for ionic composition from the 1980s baseline period. The analysis reveals significant alkalization trends across the hinterland of the Songliao Plain (Figure 12). The mean pH of saline-alkali soils increased by 0.49 units, affecting an expanded area of 3.60 million hectares since the 1980s. Notably, areas demonstrating intensified alkalization (ΔpH >0 relative to original alkaline conditions) covered 11.26 Mha, with spatial clustering in the Songliao Plain's central basin. Critical threshold analysis shows that zones with pH increases exceeding 0.75 units consistently transitioned to moderate-severe saline-alkali classifications. The extremity of soil alkalization shows particularly concerning progression: while 1980s data indicated maximum pH values of 9.8 with merely 96,000 ha (0.096 Mha) exceeding pH 9.5, contemporary measurements reveal 2.81 Mha now surpass this threshold—representing an annual expansion rate of 80,300 ha/yr in the past 4 decades. Simultaneously, we observed 5.19 Mha of acid-to-alkaline soil transition, though marginal areas near the Songliao Plain exhibited localized pH decreases (mean ΔpH -0.12), suggesting complex spatial heterogeneity in salinization drivers.

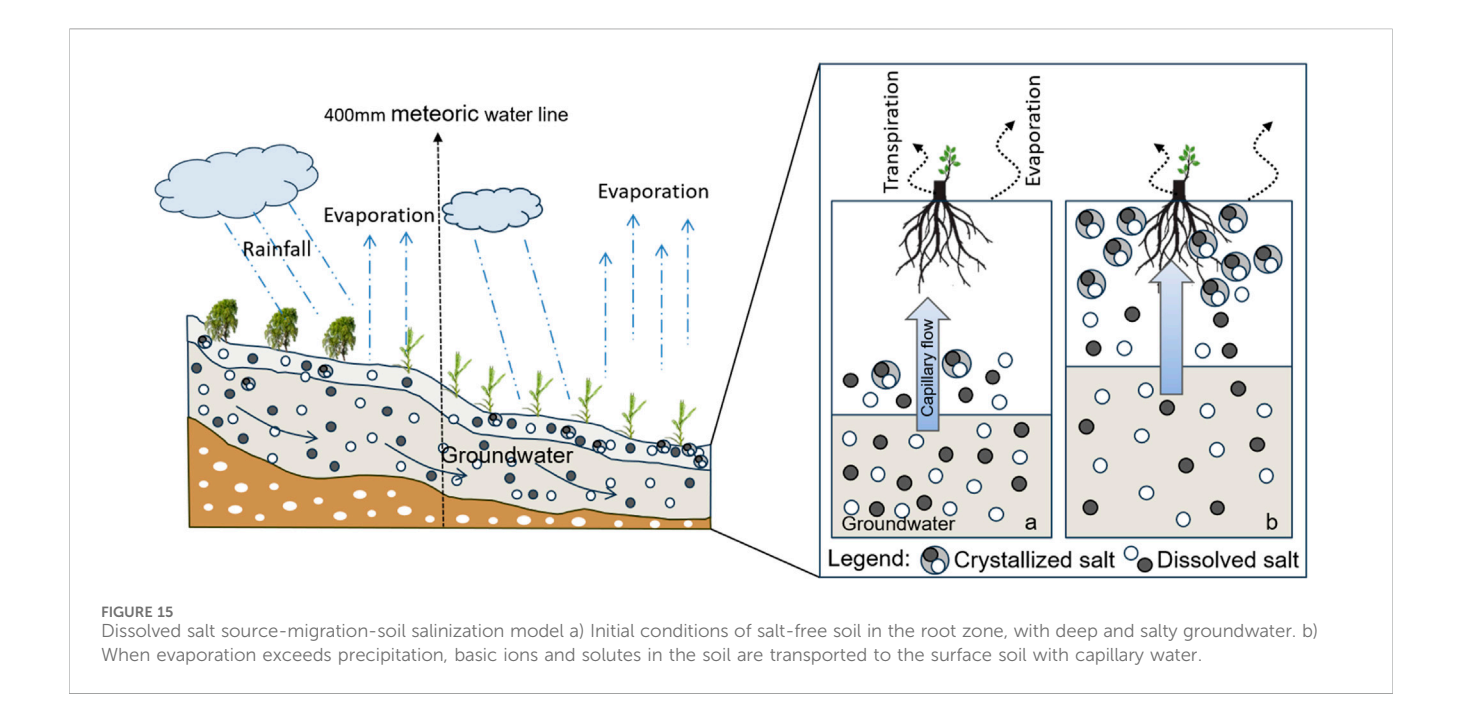
3.2.2 Driving factors of salinization

The four-decade comparative analysis of spatiotemporal pH variations reveals critical patterns in the Northeast China Plain's soil salinization. Nearly all salinized/alkalized areas (99.98%) exhibited dryness coefficients >1.0. Saline-alkali soils were mainly distributed in areas with a dryness coefficient above 1.6, particularly in the western part of the Songliao Plain. Land use analysis shows farmland constitutes 48.71% of the total area. The soil



pH of unchanged farmland increased by 0.31—lower than the change observed across the entire study area. Notably, saline-alkali lands showed greater alkalization (Δ pH +1.18) than grasslands (Δ pH +0.70). Elevation-dependent patterns emerged, with maximum pH increase (+1.0) at 140 m (Figure 13) within a characteristic inverted V-shaped distribution (100–180 m). The hydrogeochemical system features centripetal water flow (Figure 14) transporting mineral-rich sediments from the

Hinggan Mountains' granite/volcanic belts. These albite-bearing materials release Na⁺, Ca²⁺, and K⁺ through weathering, forming sulfuric acid solutions that migrate to low-lying plains (<200 m elevation). When evaporation exceeds precipitation (dryness coefficient >1.6), capillary action brings salts to surface layers, creating saline-alkali soils. Figure 15 illustrates this complete salt source-transport-precipitation (model a and b) cycle. While cultivation shows moderate mitigation effects, the interplay of



topography, hydrogeology, and climate continues driving salinization in this vulnerable ecosystem.

4 Conclussion

The Northeast China Plain contains no less than 16.93 million hectares of salinized or alkalinized zonal soils, distributed in chernozem, meadow soil, phaeozem, aeolian sand soil, and saline-alkali soil. The study reveals 6.92 million hectares of saline-alkaline soils—substantially more than remote sensing estimates. Notably, 2.89 million hectares of strongly alkaline soil (pH > 9.5) severely threatens agricultural productivity. While soils with pH > 7.5 occur locally in the Sanjiang Plain, their dryness coefficient (<1.6) and salt content (<0.3%) do not meet saline-alkali criteria. Our geochemical analysis identified pH is greater than 8.5 as one of the critical threshold for salinization indicators in surface soils (0-20 cm). These findings provide crucial data for global salinealkali soil mapping, demonstrating the Northeast China Plain's distinct distribution patterns of saline-alkali soils. Unlike remote sensing methods (based on land use, vegetation, and salinity indices), our geochemical approach effectively detects hidden saline-alkali soils and characterizes their chemistry (predominantly chloride and bicarbonate types).

In Northeast China Plain, soils with pH > 9.5 have expanded since the 1980s. Notably, the 140-m elevation zone exhibited peak values in soil pH, the magnitude of pH increase over the past 4 decades, and concentrations of salinization-related elements. Comparative analysis of cropland *versus* saline-alkali soils reveals agricultural practices significantly alter salt distribution (evident in total salts, EC, and Na⁺ patterns) but have mitigated rather than accelerated salinization. Primary drivers of salinization intensification include the synergistic effects of topography, hydrogeology, and precipitation-evaporation dynamics. Effective

saline-alkali soil management requires location-specific strategies that account for hydrogeological, meteorological, and geographical conditions.

Data availability statement

The datasets presented in this article are not readily available because The dataset can not be used. Requests to access the datasets should be directed to daihuimin78@126.com.

Author contributions

HD: Project administration, Validation, Funding acquisition, Supervision, Formal Analysis, Writing – original draft, Software, Data curation, Investigation, Writing – review and editing, Resources, Conceptualization, Visualization, Methodology. YF: Writing – review and editing, Project administration. CC: Writing – review and editing, Formal Analysis, Data curation, Methodology. KL: Data curation, Writing – review and editing, Investigation. XL: Formal Analysis, Investigation, Writing – review and editing. NF: Data curation, Writing – review and editing. YZ: Investigation, Writing – review and editing. TR: Investigation, Writing – review and editing.

Funding

The author(s) declare that financial support was received for the research and/or publication of this article. This work was supported by the Strategic Priority Research Program of the Chinese Academy of Sciences (XDA28020302), and financially supported by the National Key R&D Program of China (Grant No. 2023YFD1500801).

Conflict of interest

The authors declare that the research was conducted in the absence of any commercial or financial relationships that could be construed as a potential conflict of interest.

Generative AI statement

The author(s) declare that no Generative AI was used in the creation of this manuscript.

Any alternative text (alt text) provided alongside figures in this article has been generated by Frontiers with the support of artificial

Publisher's note

you identify any issues, please contact us.

All claims expressed in this article are solely those of the authors and do not necessarily represent those of their affiliated organizations, or those of the publisher, the editors and the reviewers. Any product that may be evaluated in this article, or claim that may be made by its manufacturer, is not guaranteed or endorsed by the publisher.

intelligence and reasonable efforts have been made to ensure accuracy, including review by the authors wherever possible. If

References

Adeyemo, T., Kramer, I., Levy, G. J., and Mau, Y. (2022). Salinity and sodicity can cause hysteresis in soil hydraulic conductivity. *Geoderma* 413, 115765. doi:10.1016/j. geoderma.2022.115765

Bao, S. (2000). Soil and agricultural chemistry analysis. 3rd ed. Beijing: China Agriculture Press.

Breiman, L. (2001). Random forests. *Mach. Learn.* 45, 5–32. doi:10.1023/A: 1010933404324

Butcher, K., Wick, A. F., Desutter, T., Chatterjee, A., and Harmon, J. (2016). Soil salinity: a threat to global food security. *Agron. J.* 108 (6), 2189–2200. doi:10.2134/agronj2016.06.0368

Chaieb, C., Abdelly, C., and Michalet, R. (2019). Interactive effects of climate and topography on soil salinity and vegetation zonation in north-African continental saline depressions. *J. Veg. Sci.* 30 (2), 312–321. doi:10.1111/jvs.12693

Chen, S., Jin, Z., Zhang, J., Chu, G., Sang, W., and Lin, H. (2020). Situation and impact factors of soil salinization in different dammed farmlands in the valley area of the Northern Shaanxi Province. *J. Earth Environ.* 11 (1), 81–89. doi:10.19678/j.issn.1000-6360.202001007

Chen, M., Kuzyakov, Y., Zhou, J., Zamanian, K., Wang, S., Abdalla, K., et al. (2025). High soil salinity reduces straw decomposition but primes soil organic carbon loss. *Soil Biol. Biochem.* 207, 109835. doi:10.1016/j.soilbio.2025.109835

Chernousenko, G. I., and Kurbatskaya, S. S. (2017). Soil salinization in different natural zones of intermontane depressions in Tuva. *Eurasian Soil Sci.* 50 (11), 1255–1270. doi:10.1134/S1064229317110047

Corwin, D. L. (2021). Climate change impacts on soil salinity in agricultural areas. Eur. J. Soil Sci. 72 (2), 842–862. doi:10.1111/ejss.13010

Dai, Y., Guan, Y., Zhang, Q., Sun, J., and He, X. (2022). Remote sensing monitoring and temporal and spatial characteristics of soil salinization in Aral Reclamation Area. *Arid. Land Geogr.* 45 (4), 1176–1185. doi:10.12118/j.issn.1000-

Daliakopoulos, I. N., Tsanis, I. K., Koutroulis, A., Kourgialas, N. N., Varouchakis, A. E., Karatzas, G. P., et al. (2016). The threat of soil salinity: a European scale review. *Sci. Total Environ.* 573, 727–739. doi:10.1016/j.scitotenv.2016.08.177

Daniels, L. W. (2016). The nature and properties of soils. Soil Sci. Soc. Am. J. 80 (5), 1428. doi:10.2136/sssaj2016.0005br

Elmeknassi, M., Elghali, A., Carvalho, H. W. P., Laamrani, A., and Benzaazoua, M. (2024). A review of organic and inorganic amendments to treat saline-sodic soils: emphasis on waste valorization for a circular economy approach. *Sci. Total Environ.* 921, 171087. doi:10.1016/j.scitotenv.2024.171087

Eswar, D., Karuppusamy, R., and Chellamuthu, S. (2021). Drivers of soil salinity and their correlation with climate change. *Curr. Opin. Environ. Sustain.* 50, 310–318. doi:10. 1016/j.cosust.2020.10.015

Food and Agriculture Organization (FAO) (2022). Global Symposium on Salt-Affected Soils: outcome document. Rome, 1–28. doi:10.4060/cb9929en

Hao, L., Ma, L., and Zhao, H. (2004). Elemental homogenization during weathering and pedogenesis of volcanic rocks from North Da Hinggan Ling. *Geochemica* 33 (2), 131–138.

Hu, Y., Yang, F., Yang, N., Jia, W., and Cui, Y. (2023). Analysis and prospects of saline-alkali land in China from the perspective of utilization. *Chin. J. Soil Sci.* 54 (2), 489–494. doi:10.19336/j.cnki.trtb.2022031902

Ivushkin, K., Bartholomeus, H., Bregt, A. K., Pulatov, A., Kempen, B., and Luis, D. S. (2019). Global mapping of soil salinity change. *Remote Sens. Environ.* 231, 111260. doi:10.1016/j.rse.2019.111260

Kirsten, B., Wick, A. F., Thomas, D. S., Amitava, C., and Jason, H. (2018). Corn and soybean yield response to salinity influenced by soil texture. *Agron. J.* 110 (4), 1243–1253. doi:10.2134/agronj2017.10.0619

Kumar, P., Tiwari, P., Biswas, A., and Srivastava, P. K. (2024). Spatio-temporal assessment of soil salinization utilizing remote sensing derivatives, and prediction modeling: Impliiations for sustainable development. *Geosci. Front.* 15 (6), 101881. doi:10.1016/j.gsf.2024.101881

Li, A., Wu, Y., and Cao, S. (2024). Effects of land use-land cover on soil water and salinity contents. *Ecol. Front.* 4 (2), 307–314. doi:10.1016/j.chnaes.2023.07.002

Lin, N., and Tang, J. (2005). Study on the environment evolution and the analysis of causes to land salinization and desertification in Songnen Plain. *J. Geogr. Sci.* 25 (4), 474–483. Available online at: http://www.dsjyj.com.cn/article/id/dsjyj_9041.

Liu, B., Huang, L., Jiang, X., Liu, Y., Huang, G., Yang, C., et al. (2024). Quantitative evaluation and mechanism analysis of soil chemical factors affecting rice yield in saline-sodic paddy fields. *Sci. Total Environ.* 929, 172584. doi:10.1016/j.scitotenv.2024.172584

Lobell, D. B. (2010). Remote sensing of soil degradation: introduction. *J. Environ. Qual.* 39, 1–4. doi:10.2134/jeq2009.0326

Lobell, D. B., Lesch, S. M., Corwin, D. L., Ulmer, M. G., Anderson, K. A., Potts, D. J., et al. (2010). Regional-scale assessment of soil salinity in the Red River Valley using multi-year MODIS EVI and NDVI. *J. Environ. Qual.* 39, 35–41. doi:10.2134/jeq2009.

Muhammad, M., Waheed, A., Wahab, A., Majeed, M., Nazim, M., Liu, Y., et al. (2024). Soil salinity and drought tolerance: an evaluation of plant growth, productivity, microbial diversity, and amelioration strategies. *Plant Stress* 11, 100319. doi:10.1016/j.stress.2023.100319

Nachshon, U. (2018). Cropland soil salinization and associated hydrology: trends, processes and examples. *Water* 10 (8), 1030. doi:10.3390/w10081030

Rengasamy, P. (2016). Soil chemistry factors confounding crop salinity tolerance—A review. *Agronomy* 6 (4), 53. doi:10.3390/agronomy6040053

Shi, X., Wang, H., Warner, E. D., Wang, H., Sun, W., Zhao, Y., et al. (2010). Cross-reference for relating Genetic Soil Classification of China with WRB at different scales. *Geoderma* 155, 344–350. doi:10.1016/j.geoderma.2009.12.017

Singh, A. (2021). Soil salinization management for sustainable development: a review. *J. Environ. Manag.* 277, 111383. doi:10.1016/j.jenvman.2020.111383

Sudhir, P., and Murthy, S. (2004). Effects of salt stress on basic processes of photosynthesis. *Photosynthetica* 42, 481–486. doi:10.1007/S11099-005-0001-6

Tedeschi, A. (2020). Irrigated agriculture on saline soils: a perspective. Agronomy 10 (11), 1630. doi:10.3390/agronomy10111630

Thorne, D. W. (1954). Diagnosis and improvement of saline and alkali soils. BioScience~4~(3),~14.~doi:10.1093/aibsbulletin/4.3.14-a

Wan, X., Gong, F., Qu, M., Qiu, E., and Zhong, C. (2019). Experimental study of the salt transfer in a cold sodium sulfate soil. *KSCE J. Civ. Eng.* 23, 1573–1585. doi:10.1007/s12205-019-0905-5

Wang, S., and Huang, Y. (2023). Research progress on saline-alkali land improvement in Songnen Plain. *Soils Crops* 12 (2), 206–217. Available online at: http://sc.iga.ac.cn/cn/article/id/f0decde5-d38f-4bd4-b6ff-3512c21adbf4.

Wang, W., Vincour, B., and Altman, A. (2003). Plant responses to drought, salinity and extreme temperatures: towards genetic engineering for stress tolerance. *Planta* 218, 1–14. doi:10.1007/s00425-003-1105-5

Wang, J., Dun, Y., Guo, Y., and Dou, S. (2014). Effects of land consolidation on improvement of salinity soil in Western Songnen Plain. *Trans. Chin. Soc. Agric.*

 $\it Eng.~33~(18),~266-275.$ Available online at: https://doc.taixueshu.com/journal/20140735nygcxb.html.

Wang, H., Zhao, L., Chen, Y., Wang, L., Zhao, X., and Sui, B. (2019). Spatio-temporal integration technology model and its mechanism of improving quality and fertility for soda saline soil in songnen Plain. *J. Jilin Agric. Univ.* 44 (6), 694–698. Available online at: http://qikan.cqvip.com/Qikan/Article/Detail?id=7109008774.

Wang, L., Wang, T., Gao, B., He, H., Ding, X., and Hou, B. (2023a). Spatiotemporal dynamics of soil salinity and its determinants in Songnen Plain. *J. Irrig. Drain.* 42 (4), 108–115. doi:10.13522/j.cnki.ggps.2022339

Wang, J., Yang, T., Zhu, K., Shao, C., Zhu, W., Hou, G., et al. (2023b). A novel retrieval model for soil salinity from CYGNSS: algorithm and test in the Yellow River Delta. *Geoderma* 432, 116417. doi:10.1016/j.geoderma.2023.116417

Wang, J., Sun, Z., Yang, T., Wang, B., Dou, W., and Zhu, W. (2024). Quantifying the effect of salinity on dielectric-based soil moisture measurements using COSMOS records. *J. Hydrology* 643, 131925. doi:10.1016/j.jhydrol.2024.131925

Weil, R. R., and Brady, N. C. (2016). *The nature and properties of soils*. 15th edition 5, 333–465. Available online at: https://api.semanticscholar.org/CorpusID:135371459.

Xing, J., Li, X., Li, Z., Wang, X., Hou, N., and Li, D. (2024). Remediation of sodasaline-alkali soil through soil amendments: microbially mediated carbon and nitrogen cycles and remediation mechanisms. *Sci. Total Environ.* 924, 171641. doi:10.1016/j. scitotenv.2024.171641

Xu, Z., and Xu, X. (2018). The cause of Formation and characteristics of soda saline-alkaline land of the songnen Plain and the Study progress of control measures. Soil

 $\label{thm:water Conserv. China 431 (2), 54-60. Available online at: https://www.doc88.com/p-15629073943326.html.$

Xu, X., Liu, S., Zhao, Y., Xu, Z., Yang, X., Teng, M., et al. (2018). Effects of different environmental factors on distribution of soda Salinie-alkaline land in Western Jilin Province. *Bull. Soil Water Conserv.* 38 (1), 89–95. Available online at: https://d.wanfangdata.com.cn/periodical/stbctb201801015.

Zhang, W., and Feng, Y. (2009). Physico-chemical properties and ecological recovery of saline-alkaline soil in Songnen Plain. *Acta Pedol. Sin.* 46 (1), 169–172. Available online at: http://pedologica.issas.ac.cn/trxb/article/abstract/2009460125.

Zhang, S., Yang, J., Li, Y., Zhang, Y., and Chang, L. (2010). Changes of saline-alkali land in Northeast China and its causes since the mid-1950s. *J. Nat. Resour.* 25 (3), 435–442. doi:10.11849/zrzyxb.2010.03.009

Zhang, Y., Li, X., Hu, H., Chen, W., and Wang, X. (2017). Research status and prospect of saline-alkaline land improvement. *Jiangsu Agric. Sci.* 45 (18), 7–10. Available online at: http://www.jsnykx.cn/oa/darticle.aspx?type=view&id=201718002

Zhao, P., and Jia, Z. (2020). Study on ecological management of saline-alkali land in west of Northeast Plain. Water Resour. and Hydropower Northeast 5 (72), 47–49. Available online at: https://d.wanfangdata.com.cn/periodical/dbslsd202005020.

Zhao, Y., Li, Y., Wang, X., Zhao, Z., Liu, X., Wang, S., et al. (2019). Research progress of element behavior in rock weathering and soil formation. *Heilongjiang Agric. Sci.* 1, 147–150. Available online at: https://d.wanfangdata.com.cn/periodical/hljnykx201901037.